

# **SANDIA REPORT**

SAND2013-2689  
Unlimited Release  
Printed March 2013

## **Source Identification in Acoustics and Structural Mechanics using SIERRA/SD**

Timothy Walsh, Wilkins Aquino, Mike Ross

Prepared by  
Sandia National Laboratories  
Albuquerque, New Mexico 87185 and Livermore, California 94550

Sandia National Laboratories is a multiprogram laboratory managed and operated by Sandia Corporation, a wholly owned subsidiary of Lockheed Martin Corporation, for the United States Department of Energy's National Nuclear Security Administration under Contract DE-AC04-94AL85000.

Approved for public release; further dissemination unlimited.



**Sandia National Laboratories**

Issued by Sandia National Laboratories, operated for the United States Department of Energy by Sandia Corporation.

**NOTICE:** This report was prepared as an account of work sponsored by an agency of the United States Government. Neither the United States Government, nor any agency thereof, nor any of their employees, nor any of their contractors, subcontractors, or their employees, make any warranty, express or implied, or assume any legal liability or responsibility for the accuracy, completeness, or usefulness of any information, apparatus, product, or process disclosed, or represent that its use would not infringe privately owned rights. Reference herein to any specific commercial product, process, or service by trade name, trademark, manufacturer, or otherwise, does not necessarily constitute or imply its endorsement, recommendation, or favoring by the United States Government, any agency thereof, or any of their contractors or subcontractors. The views and opinions expressed herein do not necessarily state or reflect those of the United States Government, any agency thereof, or any of their contractors.

Printed in the United States of America. This report has been reproduced directly from the best available copy.

Available to DOE and DOE contractors from  
U.S. Department of Energy  
Office of Scientific and Technical Information  
P.O. Box 62  
Oak Ridge, TN 37831

Telephone: (865) 576-8401  
Facsimile: (865) 576-5728  
E-Mail: [reports@adonis.osti.gov](mailto:reports@adonis.osti.gov)  
Online ordering: <http://www.osti.gov/bridge>

Available to the public from  
U.S. Department of Commerce  
National Technical Information Service  
5285 Port Royal Rd  
Springfield, VA 22161

Telephone: (800) 553-6847  
Facsimile: (703) 605-6900  
E-Mail: [orders@ntis.fedworld.gov](mailto:orders@ntis.fedworld.gov)  
Online ordering: <http://www.ntis.gov/help/ordermethods.asp?loc=7-4-0#online>



# Source Identification in Acoustics and Structural Mechanics using SIERRA/SD

Timothy Walsh  
Computational Solid Mechanics and Structural Dynamics  
Sandia National Laboratories  
P.O. Box 5800  
Albuquerque, NM 87185-0380 tfwalsh@sandia.gov

Wilkins Aquino  
Department of Civil and Environmental Engineering  
Duke University  
Durham, NC  
wilkins.aquino@duke.edu

Mike Ross  
Analytical Structural Dynamics  
Sandia National Laboratories  
P.O. Box 5800  
Albuquerque, NM 87185-0828 mross@sandia.gov

## Abstract

In this report we derive both time and frequency-domain methods for inverse identification of sources in elastodynamics and acoustics. The inverse/design problem is cast in a PDE-constrained optimization framework with efficient computation of gradients using the adjoint method. The implementation of source inversion in Sierra/SD is described, and results from both time and frequency domain source inversion are compared to actual experimental data for a weapon store used in captive carry on a military aircraft. The inverse methodology is advantageous in that it provides a method for creating ground based acoustic and vibration tests that can reduce the actual number of flight tests, and thus, saving costs and time for the program.

# Contents

1	Introduction .....	7
2	Background .....	9
2.1	Forward Problem Formulation .....	9
2.2	Inverse Problem Formulation .....	11
2.3	Regularization .....	16
3	Numerical Results on a Weapon Store .....	19
3.1	Frequency Domain Approach .....	19
3.2	Time Domain Approach .....	20
4	Conclusions .....	33
	References .....	34

# Figures

1	The acoustic mesh and structural representation of the system of interest. .	19
2	The locations of the 17 microphones where experimental data was collected. . . . .	20
3	A comparison of measured and predicted acoustic pressures (real component) from a frequency-domain solution of the source inversion problem on a system-level reverberation chamber test. Experimental and simulation results are compared at all 17 microphones at $f = 315\text{Hz}$ . . . . .	21
4	A comparison of measured and predicted acoustic pressures (imaginary component) from a frequency-domain solution of the source inversion problem on a system-level reverberation chamber test. Experimental and simulation results are compared at all 17 microphones at $f = 315\text{Hz}$ . . . . .	21
5	A comparison of measured and predicted acoustic pressures at microphones 1 and 2. . . . .	23
6	Closeup views of the time span from $t = 0.02\text{s}$ to $t = 0.1\text{s}$ of experimental and predicted acoustic pressures at microphone 1. . . . .	24
7	A comparison of experimental and predicted acoustic pressures at microphones 3 and 4. . . . .	25
8	A closeup view of the early time comparison of experimental and predicted acoustic pressures at microphones 5 and 6. . . . .	26
9	A closeup view of the early time comparison of experimental and predicted acoustic pressures at microphones 7 and 8. . . . .	27
10	A closeup view of the early time comparison of experimental and predicted acoustic pressures at microphones 9 and 10. . . . .	28
11	A closeup view of the early time comparison of experimental and predicted acoustic pressures at microphones 11 and 12. . . . .	29
12	A closeup view of the early time comparison of experimental and predicted acoustic pressures at microphones 13 and 14. . . . .	30
13	A closeup view of the early time comparison of experimental and predicted acoustic pressures at microphones 15 and 16. . . . .	31
14	A comparison of measured and predicted acoustic pressures at microphone 17. . . . .	32
15	Acoustic accelerations on first and second patches of Figure 1. . . . .	32



# 1 Introduction

Methods for source localization are of high relevance in a variety of engineering and scientific applications. The source localization challenge is often cast within the mathematical framework of an inverse problem in which we are tasked with identifying a hidden driving force given the measured response of a system. Important examples of this class of problems include earthquake source localization [1, 2], damage or defect identification from acoustic emission [3, 4, 5], odor or contaminant localization [6], acoustics [14], and source identification in electromagnetics [7], among others. In spite of the different physics involved in the latter examples, their mathematical structures share many common features, allowing us to develop methods that are applicable to a wide range of problems.

Most popular approaches used for source localization in wave propagation problems (mechanical and electromagnetic) are centered around the concept of Time Reversal (TR) [8, 7, 9]. In TR methods, by reversing time, the measured signal is back propagated through the system and energy is focused on the region where sources are located, causing their illumination. To be applicable, the TR concept requires linearity and non-lossy or slightly lossy media. It is imperative to also mention that the TR concept has a frequency domain analog called the Phase Conjugation Mirror (PCM) [10]. The TR/PCM concepts have been extended to enhance robustness via the MUSIC (MUltiple SIgnal Classification) method [11]. The MUSIC method considers the response received at each of the measurement points in series, ultimately forming a response matrix for the entire measurement array. Once the response matrix is formed, one can use a variety of robust techniques from linear algebra (*e.g.* singular value decomposition) to infer measurement locations. Holography is another technique that rests upon the same theoretical basis as TR/PCM, but makes additional assumptions about the frequency spread and/or the length scale at which measurements are made [12]. Recently, a general Bayesian framework was proposed for obtaining an optimal basis that minimize the reconstruction error in acoustic source identification problems [13]. The latter work demonstrated that this framework can be used with classical acoustic source reconstruction methods. Interestingly, the authors found that iterative optimization algorithms have not been widely used for source localization in acoustics and elastic wave propagation. This finding contrasts with the widespread use of large scale optimization theory and algorithms in other inverse problems, including source identification in contaminant transport [6]. In a related work, a stochastic PDE-constrained optimization strategy [14] was recently developed to solve source inversion problem.

At Sandia, source localization arises in various stages of qualification testing and simulation. Acoustic excitation is typically applied in reverberation or direct field acoustic testing (DFAT) in order to simulate in-service environments. Mechanical excitation is commonly applied on shaker tables to apply specified loads to components of interest. In both cases, the measured or desired profiles of point accelerations or microphone pressures are given and it is necessary to estimate the input loads (acoustic or mechanical) that reproduce these accelerations or pressures. These source inversion problems have driven the code development work described in this report.

We present in this work a PDE-constrained optimization formulation for the inverse identification of sources in elastodynamics and acoustics. We have taken this approach because it is applicable not only on linear inverse problems such as the one described in this report, but also is easily extended to problems with nonlinearities, lossy mechanisms, and large numbers of design variables. Many applications of interest include these extra complexities.

This report is organized as follows. First, we provide formulations for the forward problems (acoustics and elastodynamics) of interest. Then, the inverse/design problem is cast in a PDE-optimization framework. We provide precise details for the efficient computation of gradients using an adjoint-based approach. Furthermore, we provide details on how to treat Neumann boundary conditions as those usually encountered in force identification problems in acoustics and elastodynamics. We then provide results of a comparison between numerical results obtained from the inverse problem and actual experimental data that was recently taken while testing a weapon store in the reverberation chamber.

## 2 Background

### 2.1 Forward Problem Formulation

#### 2.1.1 Governing Equations

The strong-form of the initial-boundary value problems for solid mechanics, in the absence of body forces, is given as

$$\nabla \cdot \boldsymbol{\sigma} = \rho \ddot{\mathbf{u}}, \quad \text{in } \Omega \times (0, T) \quad (1a)$$

$$\boldsymbol{\sigma} \mathbf{n} = \mathbf{h}, \quad \text{on } \partial\Omega^N \times [0, T] \quad (1b)$$

$$\boldsymbol{\sigma} = \mathbf{D} : \nabla \mathbf{u}, \quad \text{in } \Omega \times [0, T] \quad (1c)$$

$$\mathbf{u} = \mathbf{0}, \quad \text{on } \partial\Omega^D \times [0, T] \quad (1d)$$

$$\mathbf{u}(0, T) = \mathbf{0}, \quad \text{in } \Omega \quad (1e)$$

$$\dot{\mathbf{u}}(0, T) = \mathbf{0}, \quad \text{in } \Omega \quad (1f)$$

where  $\mathbf{u}$  is displacement,  $\boldsymbol{\sigma}$  is the stress tensor,  $\rho$  is density,  $\mathbf{h}$  is a prescribed traction vector,  $\mathbf{n}$  is the unit vector normal to the boundary,  $\partial\Omega^N$  is the part of the boundary where Neumann boundary conditions are specified,  $\partial\Omega^D$  is the portion of the boundary where  $\mathbf{u}$  is specified. Notice that  $\partial\Omega^N$  and  $\partial\Omega^D$  are non-overlapping and their union is all of  $\partial\Omega$ . The variable  $\mathbf{D}$  represents the (fourth order) elasticity tensor describing the underlying material. We are representing vector and tensor-valued fields (as well as constant vectors and tensors) with bold symbols, while scalar fields and constants will be given in italics font. Derivatives are denoted with over dots.

The strong form of the acoustics problem (counterpart to the elastodynamics problem shown above) is given as

$$\nabla^2 \phi = \frac{1}{c^2} \ddot{\phi}, \quad \text{in } \Omega_f \times (0, T) \quad (2a)$$

$$\nabla \phi \cdot \mathbf{n}_f = -\rho_f \ddot{u}_n, \quad \text{on } \partial\Omega_f^N \times [0, T] \quad (2b)$$

$$\phi = 0, \quad \text{on } \partial\Omega_f^D \times [0, T] \quad (2c)$$

$$\phi(0, T) = 0, \quad \text{in } \Omega_f \quad (2d)$$

$$\dot{\phi}(0, T) = 0, \quad \text{in } \Omega_f \quad (2e)$$

where  $\phi$  is acoustic pressure,  $c$  is the wave speed of the fluid,  $\Omega_f$  is the fluid domain,  $\mathbf{n}_f$  is the unit vector normal to the surface,  $\rho_f$  is the fluid density,  $\ddot{u}_n$  is the normal particle acceleration applied over the Neumann boundary  $\partial\Omega_f^N$ , and  $\Omega_f^D$  is the Dirichlet boundary.

**Remark 1.** *Radiation conditions can be specified over part or the entire boundary in both the elastodynamics and the acoustics problems. The treatment of this type of boundary conditions can be found in Reference [15].*

### 2.1.2 Discrete Equations

For both the acoustic and structural dynamic problems, the spatial discretization of the governing equations is obtained by first constructing the variational or weak formulation of the problems described in the previous section and then introducing a finite element approximation scheme. The details of these discretization steps are not shown herein for the sake of brevity and can be found in Reference [16]. We directly state that the resulting semi-discrete system is given as

$$[M]\mathbf{a}(t) + [C]\mathbf{v}(t) + [K]\mathbf{u}(t) = \mathbf{f}(t), \quad (3)$$

where  $[M]$  is the mass matrix,  $[C]$  is the damping matrix,  $[K]$  is the stiffness matrix,  $\mathbf{a}(t)$  is the nodal acceleration vector,  $\mathbf{v}(t)$  is the nodal velocity vector,  $\mathbf{u}(t)$  is the nodal displacement vector, and  $\mathbf{f}(t)$  is the nodal force vector. Also, initial and Dirichlet conditions can be enforced in a straightforward way in Eq. (3). The semi-discrete system of equations for acoustics problems is derived in a similar manner and details of this type of problems will be omitted from hereon.

Equation (3) can be represented in the frequency-domain by taking the Fourier transform of both sides of the equation to get

$$[H(\omega)]\mathbf{z}(\omega) = \mathbf{F}(\omega), \quad (4)$$

where  $[H(\omega)]$  is the matrix form of the Helmholtz operator given as

$$[H(\omega)] = -\omega^2[M] + i\omega[C] + [K]. \quad (5)$$

In the above equation,  $\mathbf{z}(\omega)$  and  $\mathbf{F}(\omega)$  are the Fourier transforms of the nodal displacements,  $\mathbf{u}(t)$ , and force vector,  $\mathbf{f}(t)$ , respectively.

### 2.1.3 Time Integration

We used the Newmark Beta method for the time integration of the semi-discrete equations of motion, Eq. (3). In the sequel, we will use the parameter set  $\{\mathbf{p}\} = \{\mathbf{p}_k : \mathbf{p}_k \in \mathbb{R}^d, k = 1, \dots, P\}$  as an argument of the forcing function. In this set,  $d$  represents spatial dimension and  $P$  is the number of vectors used in the representation of the forcing function. This parameter set will be described in more detail in a later section. The governing system of equations at time  $t_{k+1}$  is given as

$$[M]\mathbf{a}_{k+1} + [C]\mathbf{v}_{k+1} + [K]\mathbf{u}_{k+1} = \mathbf{f}_{k+1}(\{\mathbf{p}\}), \quad (6)$$

while the Newmark-beta transition equations are given as

$$\mathbf{u}_{k+1} = \mathbf{u}_k + \Delta t \mathbf{v}_k + \frac{\Delta t^2}{2} [(1 - 2\beta)\mathbf{a}_k + 2\beta\mathbf{a}_{k+1}], \quad (7)$$

$$\mathbf{v}_{k+1} = \mathbf{v}_k + \Delta t [(1 - \gamma)\mathbf{a}_k + \gamma\mathbf{a}_{k+1}], \quad (8)$$

where  $\gamma$  and  $\beta$  are user-defined parameters. Further details on the implementation of this time integration scheme can be found in References [15, 16].

## 2.2 Inverse Problem Formulation

### 2.2.1 Time Domain

We will work with a fully discrete space-time (or space-frequency) formulation. Let  $\{\mathbf{d}(\{\mathbf{p}\})\} = \{\{\mathbf{u}\}, \{\mathbf{v}\}, \{\mathbf{a}\}\}$  represent the discrete dynamic response of the system. Where,  $\{\mathbf{u}\} = \{\mathbf{u}_k\}_{k=1}^N$ ,  $\{\mathbf{v}\} = \{\mathbf{v}_k\}_{k=1}^N$ , and  $\{\mathbf{a}\} = \{\mathbf{a}_k\}_{k=1}^N$ . Here  $N$  is used to denote the number of time steps of data in the time histories. Assuming that we have a measured displacement history (e.g.  $\mathbf{u}_{m_1} \dots \mathbf{u}_{m_N}$ ), we define an objective function  $J: \mathbb{R}^l \times \mathbb{R}^P \rightarrow \mathbb{R}$  as

$$J(\{\mathbf{u}\}, \{\mathbf{p}\}) = \frac{\kappa}{2} \left( \{\mathbf{u}\} - \{\mathbf{u}_m\} \right)^T [\mathcal{Q}] \left( \{\mathbf{u}\} - \{\mathbf{u}_m\} \right) + \mathcal{R}(\{\mathbf{p}\}), \quad (9)$$

where  $[\mathcal{Q}]$  is a general weight matrix (or a boolean matrix to select a subset of measured degrees of freedom),  $\kappa$  is a scaling constant,  $l$  is the number of degrees of freedom in the system times the number of time steps, and  $\mathcal{R}: \mathbb{R}^P \rightarrow \mathbb{R}$  is a regularization operator. Notice that we are using the notation  $\{\mathbf{u}\} = \{\mathbf{u}_0, \mathbf{u}_1, \dots, \mathbf{u}_N\}$  to describe the displacement history.

The source identification problem addressed herein is cast as an optimization problem as

$$\begin{aligned} & \underset{\{\mathbf{p}\}, \{\mathbf{u}\}}{\text{minimize}} && J(\{\mathbf{u}\}, \{\mathbf{p}\}) \\ & \text{subject to} && \text{Eqs (6)-(8)} \\ & && \text{and } g_i(\{\mathbf{p}\}) \leq 0, \quad i = 1 \dots n, \end{aligned} \quad (10)$$

where the inequalities  $g_i(\{\mathbf{p}\}) \leq 0$  can be, for instance, box constraints. We can express the above optimization problem in a reduced form in which only the parameters in the set  $\{\mathbf{p}\}$  are the design variables. To this end, we first notice that for a given parameter set  $\{\mathbf{p}\}$  there is a unique displacement history  $\{\mathbf{u}(\{\mathbf{p}\})\}$  (from the properties of our forward dynamics problem and the time integration algorithm used). Then, we can define a new objective function  $\tilde{J}(\{\mathbf{p}\}) \equiv J(\{\mathbf{u}(\{\mathbf{p}\})\}, \{\mathbf{p}\})$ . Using this objective function, we define a reduced optimization problem as

$$\begin{aligned} & \underset{\{\mathbf{p}\}}{\text{minimize}} && \tilde{J}(\{\mathbf{p}\}) \\ & \text{subject to} && \\ & && g_i(\{\mathbf{p}\}) \leq 0, \quad i = 1 \dots n. \end{aligned} \quad (11)$$

There is a large variety of gradient-based methods that can be used to solve the optimization problem shown in (11) (see Reference [17]). We will assume that we are interfacing with an external optimization package that requires us to supply only the computation of the objective function and its gradient (e.g. for quasi-newton methods). Therefore, our main task herein will be to devise an efficient strategy for evaluating the objective function,  $\tilde{J}(\{\mathbf{p}\})$  and its reduced gradient,  $\nabla_{\{\mathbf{p}\}} \tilde{J}$ . Second order optimization algorithms such as Newton's method, for which we would require the calculation of a Hessian, will be considered in future work. Also, a detailed discussion of optimization algorithms is outside

the scope of this report and the interested reader can consult Reference [17] for further information to this end.

## 2.2.2 Calculation of the Gradient using an Adjoint-Based Technique

We will use a Lagrangian-based approach to derive the gradient  $\nabla_{\{\mathbf{p}\}}\tilde{J}$ . For notational convenience, we will represent the discrete dynamical response of the system for a given  $\{\mathbf{p}\}$  as  $\{\mathbf{d}(\{\mathbf{p}\})\}$ . Also, we introduce a corresponding set of Lagrange multipliers as  $\{\hat{\mathbf{d}}\} = \{\{\hat{\mathbf{u}}\}, \{\hat{\mathbf{v}}\}, \{\hat{\mathbf{a}}\}\}$ . From now on, we will suppress the dependence of the dynamical response on the parameter set  $\{\mathbf{p}\}$  for simplicity. We proceed by defining a Lagrange operator as

$$\begin{aligned} \mathcal{L}(\{\mathbf{d}\}, \{\hat{\mathbf{d}}\}, \{\mathbf{p}\}) &= \tilde{J}(\{\mathbf{p}\}) + \hat{\mathbf{u}}_0^T \left( [M]\mathbf{a}_0 + [C]\mathbf{v}_0 + [K]\mathbf{u}_0 - \mathbf{f}_0(\{\mathbf{p}\}) \right) \\ &+ \sum_{k=1}^N \left\{ \hat{\mathbf{u}}_k^T \left( [M]\mathbf{a}_k + [C]\mathbf{v}_k + [K]\mathbf{u}_k - \mathbf{f}_k(\{\mathbf{p}\}) \right) \right. \\ &\quad + \hat{\mathbf{v}}_k^T [M] \left( \mathbf{v}_k - \mathbf{v}_{k-1} - \Delta t [(1-\gamma)\mathbf{a}_{k-1} + \gamma\mathbf{a}_k] \right) \\ &\quad \left. + \hat{\mathbf{a}}_k^T [M] \left( \mathbf{u}_k - \mathbf{u}_{k-1} - \Delta t \mathbf{v}_{k-1} - \frac{\Delta t^2}{2} [(1-2\beta)\mathbf{a}_{k-1} + 2\beta\mathbf{a}_k] \right) \right\}, \end{aligned} \tag{12}$$

where the equilibrium and transition equations have been included (through the use of Lagrange multipliers). Notice that since the governing equations are satisfied for a given choice of  $\{\mathbf{p}\}$ , we have  $\mathcal{L}(\{\mathbf{d}\}, \{\hat{\mathbf{d}}\}, \{\mathbf{p}\}) = \tilde{J}(\{\mathbf{p}\})$  for any choice of Lagrange multipliers  $\{\hat{\mathbf{d}}\}$ . Hence,  $\nabla_{\{\mathbf{p}\}}\tilde{J}(\{\mathbf{p}\}) = \nabla_{\{\mathbf{p}\}}\mathcal{L}(\{\mathbf{d}\}, \{\hat{\mathbf{d}}\}, \{\mathbf{p}\})$ . Using this fact, we can conveniently derive the desired gradient. To this end, we introduce the following adjoint problem.

**The Adjoint Problem** Taking variations of  $\mathcal{L}(\{\mathbf{d}\}, \{\hat{\mathbf{d}}\}, \{\mathbf{p}\})$  with respect to the dynamical response  $\{\mathbf{d}\}$  as  $\nabla_{\{\mathbf{d}\}}\mathcal{L} \cdot \{\delta\mathbf{d}\}$ , yields

$$\nabla_{\mathbf{a}_0}\mathcal{L} \cdot \delta\mathbf{a}_0 = \delta\mathbf{a}_0^T \left( [M]\hat{\mathbf{u}}_0 - \frac{\Delta t^2}{2}(1-2\beta)[M]\hat{\mathbf{a}}_1 - \Delta t(1-\gamma)[M]\hat{\mathbf{v}}_1 \right), \quad (13a)$$

$$\nabla_{\mathbf{u}_k}\mathcal{L} \cdot \delta\mathbf{u}_k = \delta\mathbf{u}_k^T \left( [M](\hat{\mathbf{a}}_k - \hat{\mathbf{a}}_{k+1}) + [K]\hat{\mathbf{u}}_k + \kappa[Q](\mathbf{u}_k - \mathbf{u}_{m_k}) \right), \quad (13b)$$

$$\nabla_{\mathbf{v}_k}\mathcal{L} \cdot \delta\mathbf{v}_k = \delta\mathbf{v}_k^T \left( [C]\hat{\mathbf{u}}_k - \Delta t[M]\hat{\mathbf{a}}_{k+1} + [M]\hat{\mathbf{v}}_k - [M]\hat{\mathbf{v}}_{k+1} \right), \quad (13c)$$

$$\nabla_{\mathbf{a}_k}\mathcal{L} \cdot \delta\mathbf{a}_k = \delta\mathbf{a}_k^T \left( [M]\hat{\mathbf{u}}_k - \beta\Delta t^2[M]\hat{\mathbf{a}}_k - \frac{\Delta t^2}{2}[M](1-2\beta)\hat{\mathbf{a}}_{k+1}, \quad (13d)$$

$$-\Delta t[M](\gamma\hat{\mathbf{v}}_k + (1-\gamma)\hat{\mathbf{v}}_{k+1}) \right), \quad (13e)$$

$$\nabla_{\mathbf{u}_N}\mathcal{L} \cdot \delta\mathbf{u}_N = \delta\mathbf{u}_N^T \left( [M]\hat{\mathbf{a}}_N + [K]\hat{\mathbf{u}}_N + \kappa[Q](\mathbf{u}_N - \mathbf{u}_{m_N}) \right), \quad (13f)$$

$$\nabla_{\mathbf{v}_N}\mathcal{L} \cdot \delta\mathbf{v}_N = \delta\mathbf{v}_N^T \left( [C]\hat{\mathbf{u}}_N + [M]\hat{\mathbf{v}}_N \right), \quad (13g)$$

$$\nabla_{\mathbf{a}_N}\mathcal{L} \cdot \delta\mathbf{a}_N = \delta\mathbf{a}_N^T \left( [M]\hat{\mathbf{u}}_N - \Delta t^2\beta[M]\hat{\mathbf{a}}_N - \Delta t\gamma[M]\hat{\mathbf{v}}_N \right). \quad (13h)$$

Setting the above expressions to zero for arbitrary values of the variations, we get the following backward time stepping equations, which constitute what we call the adjoint problem.

(i) Final conditions

$$[C]\hat{\mathbf{u}}_N + [M]\hat{\mathbf{v}}_N = \mathbf{0} \quad (14a)$$

$$\hat{\mathbf{u}}_N = \Delta t^2\beta\hat{\mathbf{a}}_N + \Delta t\gamma\hat{\mathbf{v}}_N \quad (14b)$$

$$[M]\hat{\mathbf{a}}_N + [K]\hat{\mathbf{u}}_N = \kappa[Q](\mathbf{u}_{m_N} - \mathbf{u}_N) \quad (14c)$$

(ii) Backward transition equations

$$\hat{\mathbf{u}}_k - \beta\Delta t^2\hat{\mathbf{a}}_k - \Delta t\gamma\hat{\mathbf{v}}_k = \frac{\Delta t^2}{2}(1-2\beta)\hat{\mathbf{a}}_{k+1} + \Delta t(1-\gamma)\hat{\mathbf{v}}_{k+1} \quad (14d)$$

$$[C]\hat{\mathbf{u}}_k + [M](\hat{\mathbf{v}}_k - \Delta t\hat{\mathbf{a}}_{k+1} - \hat{\mathbf{v}}_{k+1}) = \mathbf{0} \quad (14e)$$

$$[M]\hat{\mathbf{a}}_k + [K]\hat{\mathbf{u}}_k = [M]\hat{\mathbf{a}}_{k+1} + \kappa[Q](\mathbf{u}_{m_k} - \mathbf{u}_k) \quad (14f)$$

(iii) Last transition equation

$$\hat{\mathbf{u}}_0 = \frac{\Delta t^2}{2}(1-2\beta)\hat{\mathbf{a}}_1 + \Delta t(1-\gamma)\hat{\mathbf{v}}_1 \quad (14g)$$

In summary, the adjoint problem allows us to obtain Lagrange multipliers  $\{\hat{\mathbf{d}}\}$  that satisfy the equation  $\nabla_{\{\mathbf{d}\}}\mathcal{L} = \mathbf{0}$ .

**The Gradient Equation** Taking a variation of the Lagrange operator with respect to the parameter set  $\{\mathbf{p}\}$ , we get

$$\nabla_{\{\mathbf{p}\}}\mathcal{L}(\{\mathbf{d}\},\{\hat{\mathbf{d}}\},\{\mathbf{p}\})\cdot\{\delta\mathbf{p}\}=\nabla_{\{\mathbf{d}\}}\mathcal{L}\cdot\{\delta\mathbf{d}\}+\nabla_{\{\mathbf{p}\}}\mathcal{L}\cdot\{\delta\mathbf{p}\}, \quad (15)$$

where we have used the chain rule of differentiation, and

$$\{\delta\mathbf{d}\}=\nabla_{\{\mathbf{p}\}}\{\mathbf{d}\}\cdot\{\delta\mathbf{p}\} \quad (16)$$

in the first term. Recall that the solution to the adjoint problem is a set of Lagrange multipliers  $\{\hat{\mathbf{d}}\}$  that satisfy  $\nabla_{\{\mathbf{d}\}}\mathcal{L}=\mathbf{0}$ . Hence, using Lagrange multipliers that are a solution to the adjoint problem, the first term of Eq. (15) is zero. Then, using these Lagrange multipliers, we can obtain the expression of the reduced gradient from Eq. (15) and Eq. (12) as

$$\nabla_{\{\mathbf{p}\}}\tilde{\mathcal{J}}=\nabla_{\{\mathbf{p}\}}\mathcal{L}=-\sum_{k=1}^N\hat{\mathbf{u}}_k^T\left(\nabla_{\{\mathbf{p}\}}\mathbf{f}_k(\{\mathbf{p}\})\right)+\nabla_{\{\mathbf{p}\}}\mathcal{R}. \quad (17)$$

In summary, the steps to evaluate the cost function and its gradient for a given set of parameters  $\{\mathbf{p}\}$  are:

1. Obtain  $\{\mathbf{d}\}$  by solving the forward governing equations Eq. (6)-(8).
2. Obtain  $\{\hat{\mathbf{d}}\}$  by solving the adjoint problem in Eqs. (14a)-(14g).
3. Evaluate the cost function  $\tilde{\mathcal{J}}$  using Eq. (9).
4. Evaluate the gradient  $\nabla_{\{\mathbf{p}\}}\tilde{\mathcal{J}}$  using Eq. (17).

### 2.2.3 Treatment of Neumann Boundary Conditions

Assume that the force vector at time  $k$  is given as

$$\mathbf{f}_k=\mathbf{f}(t_k)=\int_{\Gamma_N}[N]^T\mathbf{v}(\mathbf{x},t_k)d\Gamma_N. \quad (18)$$

For instance, in the above expression  $\mathbf{v}(\mathbf{x},t_k)=v(t_k)\mathbf{n}(\mathbf{x})$  can be the normal velocity specified over the boundary in an acoustics problem. It can also represent the surface traction in a structural problem. Furthermore, this formulation would also work for structural acoustics problem in which we could have both acoustic and structural loads.

We are interested in estimating the function  $\mathbf{v}(\mathbf{x},t)$ . We could consider the general case where this function is approximated using a finite element interpolation in space and

time. However, for the sake of brevity we will consider a particular case in which the spatial variation of the load is prescribed by a set of patches on the surface. Furthermore, the direction of the load over individual patches is assumed to be known, leaving as the main unknown a function of time over each patch. The main goal is to derive concrete expressions for the gradient of the Lagrangian with respect to the unknown parameters.

Now assume that we have a partition of the Neumann boundary  $\Gamma_N$  (*i.e.* we have partitioned it into patches). This partitioning of the boundary is expressed as

$$\Gamma_N = \bigcup_{j=1}^M \Gamma_{N_j}, \quad (19)$$

and

$$\Gamma_{N_j} \cap \Gamma_{N_l} = \emptyset \text{ for } j \neq l.$$

SIERRA/SD uses a load representation in which the direction of the load is fixed and the change of its magnitude with time or frequency is specified through a scalar function over each partition. The load can then be represented as

$$\mathbf{v}(\mathbf{x}, t) = \sum_{j=1}^M \chi_{\Gamma_{N_j}}(\mathbf{x}) \mathbf{g}_j h_j(t), \quad (20)$$

where  $\mathbf{g}_j$  is a given load direction on the  $j^{\text{th}}$  partition and  $h_j(t)$  defines the time dependency of the load over this partition. Also, we have used the characteristic function

$$\chi_{\Gamma_{N_j}}(\mathbf{x}) = \begin{cases} 1 & \mathbf{x} \in \Gamma_{N_j} \\ 0 & \text{otherwise.} \end{cases}$$

The functions  $h_j$  are taken as expansions of the form

$$h_j(t) = \sum_{q=1}^P p_q^j \phi_q(t), \quad (21)$$

where  $p_q^j, q = 1, \dots, P$  are unknown parameters corresponding to partition (patch)  $j$  and that act as coefficients of the the basis function  $\phi_q(t)$ . Then, the force vector can be parameterized by the unknowns  $\{\mathbf{p}\}$  (grouping all parameters in a vector).

Notice that for the present case the coefficients  $p_q^j$  are scalars. Now, the gradient of the Lagrangian with respect to the unknown parameters in  $\{\mathbf{p}\}$  can be determined. Using Eq. (20) and (21) with Eq. (18), the derivative of the force vector with respect to the unknown coefficients can be obtained as

$$\frac{\partial \mathbf{f}(t)}{\partial p_q^j} = \int_{\Gamma_{N_j}} [N]^T \mathbf{g}_j \phi_q(t) d\Gamma_{N_j}. \quad (22)$$

The gradient of the Lagrangian with respect to the unknown coefficients is obtained by substituting Eq. (22) into Eq. (17) to get

$$\frac{\partial \mathcal{L}}{\partial p_q^j} = - \sum_{k=1}^N \hat{\mathbf{u}}_k^T \left( \frac{\partial \mathbf{f}_k(\{p\})}{\partial p_q^j} \right) + \frac{\partial \mathcal{R}}{\partial p_q^j} \quad (23)$$

$$= - \sum_{k=1}^N \int_{\Gamma_{N_j}} \hat{\mathbf{u}}_k^T [N]^T \mathbf{g}_j \phi_q(t_k) d\Gamma_{N_j} + \frac{\partial \mathcal{R}}{\partial p_q^j} \quad (24)$$

$$= - \sum_{k=1}^N \int_{\Gamma_{N_j}} \hat{\mathbf{u}}^T(\mathbf{x}, t_k) \mathbf{g}_j \phi_q(t_k) d\Gamma_{N_j} + \frac{\partial \mathcal{R}}{\partial p_q^j}. \quad (25)$$

For the case where the basis functions  $\phi_q$  are interpolants and  $P = N$ , the gradient of the Lagrangian becomes

$$\frac{\partial \mathcal{L}}{\partial p_q^j} = - \int_{\Gamma_{N_j}} \hat{\mathbf{u}}^T(\mathbf{x}, t_q) \mathbf{g}_j d\Gamma_{N_j} + \frac{\partial \mathcal{R}}{\partial p_q^j}. \quad (26)$$

**Remark 2.** For acoustics problems,  $\mathbf{g}_j$  is the normal vector on Partition  $j$ . Since we can directly specify the scalar (normal) velocity and acceleration, there is no need to multiply by the normal in acoustic problems.

## 2.3 Regularization

The inverse problem at hand is in general ill-posed. The regularization operator introduced in a previous section is meant to address this issue. In this section, we will derive a specific form for this operator. It is important to bear in mind that there are other methodologies for regularization such as early stoppage and coarsening of the solution space, but we will restrict our attention to the penalty-like forms such as that used in Eq. (9). The simplest forms of the regularization operator are of the Tikhonov type although other forms such as total variation are also possible. In the Tikhonov approach, one uses Sobolev norms, in general, as the regularization operator. Specifically, given functions  $h_j(t)$ , we will define

$$\hat{\mathcal{R}}(\{h\}) = \frac{\alpha}{2} \sum_{j=1}^M (h_j, h_j), \quad (27)$$

where  $\alpha$  is a regularization parameter to be determined. Given approximations of the form in Eq. (21), the regularization operator can be expressed in term of the unknown coefficients as

$$\hat{\mathcal{R}}(h_1(\{p\}_1), \dots, h_M(\{p\}_M)) = \mathcal{R}(\{p\}_1, \dots, \{p\}_M) = \frac{\alpha}{2} \sum_{j=1}^M \{p\}_j^T (\{\phi\}, \{\phi\}^T) \{p\}_j, \quad (28)$$

where  $(\cdot, \cdot)$  is an inner product defined according to the type of regularization used (e.g. contains first derivatives when the  $H^1(0, t_f)$  space is used).

Let's now derive an expression for the derivative of the regularization operator with respect to the unknown parameters. This is simply obtained as

$$\frac{\partial \mathcal{R}}{\partial p_q^r} = \frac{\partial}{\partial p_q^r} \frac{\alpha}{2} \sum_{j=1}^M \{p\}_j^T (\{\phi\}, \{\phi\}^T) \{p\}_j \quad (29)$$

$$= \alpha \{p\}_r^T (\{\phi\}, \phi_q) \quad (30)$$

$$= \alpha (h_r, \phi_q). \quad (31)$$

In the case where the regularization operator is defined with the  $L^2$  inner product, the above inner product is given as

$$(h_r, \phi_q) = \int_0^{t_f} h_r(t) \phi_q(t) dt, \quad (32)$$

which can be expressed as

$$(h_r, \phi_q) = [W] \{p\}_r, \quad (33)$$

where the entries of the matrix  $[W]$  are

$$W_{ij} = \int_0^{t_f} \phi_i(t) \phi_j(t) dt.$$

As a simplification, we may use  $[W] = [I]$  where  $[I]$  is the identity matrix. The latter corresponds to the case where the  $\ell_2$  space is used as opposed to  $L^2$ . In this case, the gradient of the regularization operator simplifies to

$$\frac{\partial \mathcal{R}}{\partial p_q^r} = \alpha p_q^r. \quad (34)$$

### 2.3.1 Frequency Domain Equations

The same approach used to derive the gradient of the objective function in the time domain can be used to arrive at counterpart equations in the frequency domain. We will provide just a summary of these equations in this report as the derivations and arguments presented in the previous section carry in a straightforward way to the frequency domain. We will work with complex-valued functions in the frequency domain. Therefore, the objective function to be minimized is

$$\tilde{J}(\{\mathbf{p}\}) = \frac{\kappa}{2} \sum_{k=1}^N (\mathbf{z}_k - \mathbf{z}_{m_k})^h [Q] (\mathbf{z}_k - \mathbf{z}_{m_k}) + \mathcal{R}(\{\mathbf{p}\}), \quad (35)$$

where  $\mathbf{h}$  denotes the complex-conjugate transpose operation, and we denote as  $\{\mathbf{z}(\{\mathbf{p}\})\}$  the solution to the Helmholtz problem in Eq. (4) corresponding to a given  $\{\mathbf{p}\}$  for all frequencies.

For the frequency domain case, the Lagrangian is constructed using the real part of the forward problem as

$$\mathcal{L}(\{\mathbf{z}\}, \{\hat{\mathbf{z}}\}, \{\mathbf{p}\}) = \tilde{J}(\{\mathbf{p}\}) + \sum_{j=1}^N \text{Re} \left( \hat{\mathbf{z}}_j^{\mathbf{h}} \left( [H(\omega_j)] \mathbf{z}_j - \{F(\{\mathbf{p}\})\}_j \right) \right), \quad (36)$$

where  $\hat{\mathbf{z}}_j$  is a Lagrange multiplier corresponding to frequency step  $j$ . Using the same approach as we used in the time domain, we introduce an adjoint problem for the frequency domain case as

$$[H(\omega_j)] \overline{\hat{\mathbf{z}}_j} = \kappa [Q] \overline{(\mathbf{z}_{m_j} - \mathbf{z}_j)}, \quad (37)$$

where the overline denotes complex conjugation. Recall that this adjoint problem, for given  $\{\mathbf{z}\}, \{\mathbf{p}\}$ , is equivalent to  $\nabla_{\{\mathbf{z}\}} \mathcal{L}(\{\mathbf{z}\}, \{\hat{\mathbf{z}}\}, \{\mathbf{p}\}) = \mathbf{0}$ . Recall that for  $\{\mathbf{z}\}$  satisfying Eq. (4), and  $\{\hat{\mathbf{z}}\}$  the corresponding solution to the adjoint problem, Eq. (37), we have  $\nabla_{\{\mathbf{p}\}} \tilde{J}(\{\mathbf{p}\}) = \nabla_{\{\mathbf{p}\}} \mathcal{L}(\{\mathbf{z}\}, \{\hat{\mathbf{z}}\}, \{\mathbf{p}\})$ . Using the latter, we can then arrive at an expression for the gradient in the frequency domain. The reduced gradient with respect to the real part of  $\{\mathbf{p}\}$  is given as

$$\nabla_{\text{Re}(\{\mathbf{p}\}_k)} \tilde{J}(\{\mathbf{p}\}) = -\text{Re} \int_{\Gamma_{N_k}} \mathbf{g}_k^T \hat{\mathbf{z}}_j(\mathbf{x}) d\Gamma_{N_k} + \nabla_{\text{Re}(\{\mathbf{p}\}_k)} \mathcal{R}, \quad (38)$$

while the imaginary part is given as

$$\nabla_{\text{Im}(\{\mathbf{p}\}_k)} \tilde{J}(\{\mathbf{p}\}) = -\text{Im} \int_{\Gamma_{N_k}} \mathbf{g}_k^T \hat{\mathbf{z}}_j(\mathbf{x}) d\Gamma_{N_k} + \nabla_{\text{Im}(\{\mathbf{p}\}_k)} \mathcal{R}. \quad (39)$$

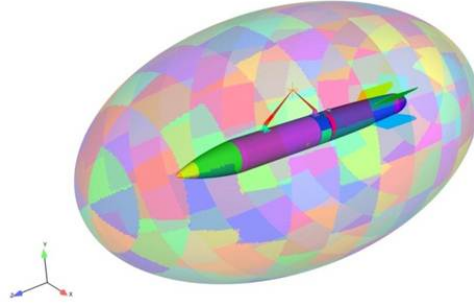


**Figure 1.** The acoustic mesh and structural representation of the system of interest.

### 3 Numerical Results on a Weapon Store

In this section, we describe the results that have been obtained on a source inversion problem involving a weapon store flown on a military aircraft. Figure 1 shows the geometry of the problem of interest. It consists of an ellipsoidal-shaped domain, with an outer surface that is divided into 171 patches. Acoustic acceleration inputs will be applied at each of these patches. Figure 2 shows the locations of the 17 microphones where the experimental measurements of acoustic pressure were taken. The goal is to come up with a set of patch accelerations that will produce the best match possible with the measured microphone pressures. We use both the time and frequency domain source inversion methodologies described in the previous sections to accomplish this goal. It is important to mention that the Barzilai-Borwein (BB) optimization algorithm from the Rapid Optimization Package (ROL), which is part of Trilinos[18], was used to obtain the results shown in this section.

**Remark 3.** *The results shown in this section correspond to an acoustics problem. We have also extensively tested the formulations and algorithms shown in previous sections in structural problems. Notice that the inverse problem formulation and algorithms shown in previous sections apply.*

#### 3.1 Frequency Domain Approach

In the case of the frequency-domain inversion, we minimize Equation (35). In order to demonstrate the effectiveness of the implementation, we took Fourier transforms of the measured time history data at the microphone locations shown in Figure 2, and then used the frequency domain source inversion methodology in Sierra/SD to solve the inverse problem by minimizing Equation (35) at the single frequency of  $f = 315\text{Hz}$ . The result was a set of patch inputs on the 171 surface patches shown in Figure 1. Using the converged set of

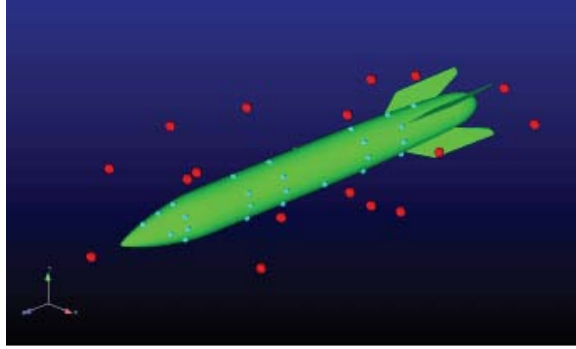


**Figure 2.** The locations of the 17 microphones where experimental data was collected.

patch inputs from the inverse problem, we ran a forward Helmholtz problem at  $f = 315\text{Hz}$  and compared the real and imaginary parts of the acoustic pressure at the microphone locations shown in Figure 2. Figures 3 and 4 show the comparisons between the experimental data and the simulation results. Good agreement is observed. This simulation was performed on 128 cores on Glory. Glory is a high performance computing platform at Sandia National Laboratories. However, due to the expense of the Helmholtz solves for the forward and adjoint problems in the inverse iterations, this inverse problem took several hours to run.

We note from equations (36) and (37) that this approach will require multiple Helmholtz solves at each frequency. With a broadband set of experimental data such as this, the expense of the Helmholtz solves at each frequency point and the number of frequency points that are required (about 700), the frequency domain approach would lead to a very computationally expensive inverse problem. For a problem that had a more narrow band of interest on the frequency axis, it is likely that the frequency-domain approach would be more efficient than the time-domain. Since the frequency range of interest for the system is so broad, we have found that the time domain approach is the most efficient approach for this problem.

### 3.2 Time Domain Approach

In the time-domain, we solve the problem described in (11). We note from equations (14) that this will involve forward and backward time-marching solutions. We take a time step equal to the inverse of the sampling frequency of the experimental data, or  $\frac{1}{25600} = 3.9063e^{-05}$ . Each of these solutions takes about half an hour on 128 cores on glory. In order to determine the time-span required for the transient solutions, we consider the lowest frequency of interest, 40Hz. If we sweep out 6 cycles at this frequency, then it will require  $\frac{6}{40} = 0.15$  seconds of time history, which corresponds to about 4000 time steps. This

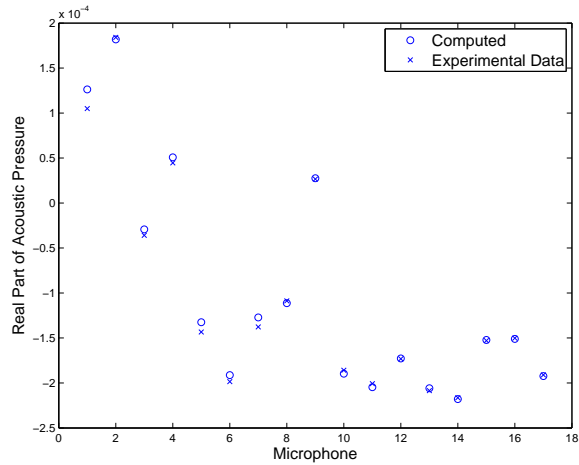


**Figure 3.** A comparison of measured and predicted acoustic pressures (real component) from a frequency-domain solution of the source inversion problem on a system-level reverberation chamber test. Experimental and simulation results are compared at all 17 microphones at  $f = 315\text{Hz}$ .

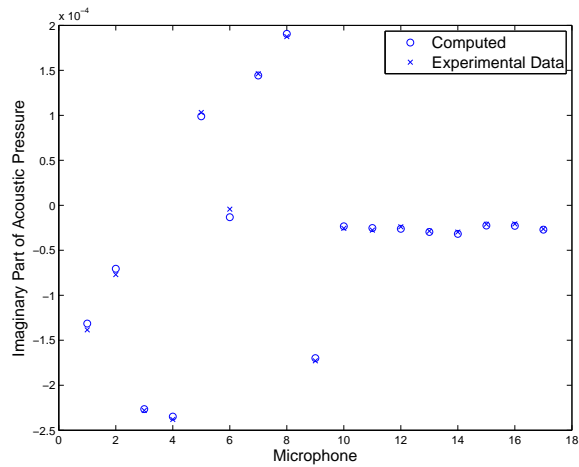


**Figure 4.** A comparison of measured and predicted acoustic pressures (imaginary component) from a frequency-domain solution of the source inversion problem on a system-level reverberation chamber test. Experimental and simulation results are compared at all 17 microphones at  $f = 315\text{Hz}$ .

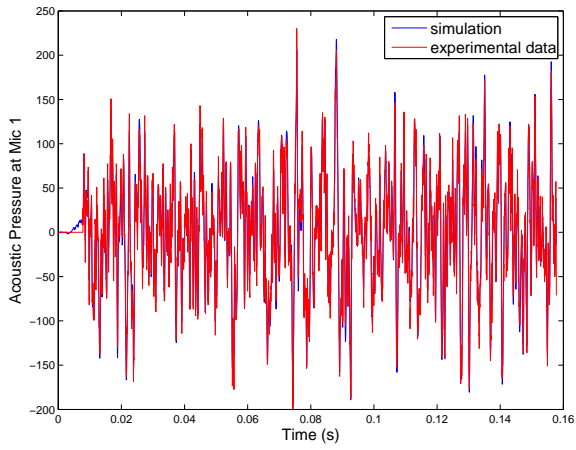
number of time steps will be required for both the forward and adjoint problems in each iteration of the inverse problem.

In order to produce a set of patch inputs that reproduce the experimental data, the source inverse methodology in Sierra/SD described in the previous sections was used to solve the inverse problem. Given these patch inputs, we then ran the forward problem described by the time-domain acoustic equation (see Equation (3)) with those inputs and wrote the microphone pressures to a history file. This allowed for a direct comparison of the predicted and measured microphone pressures.

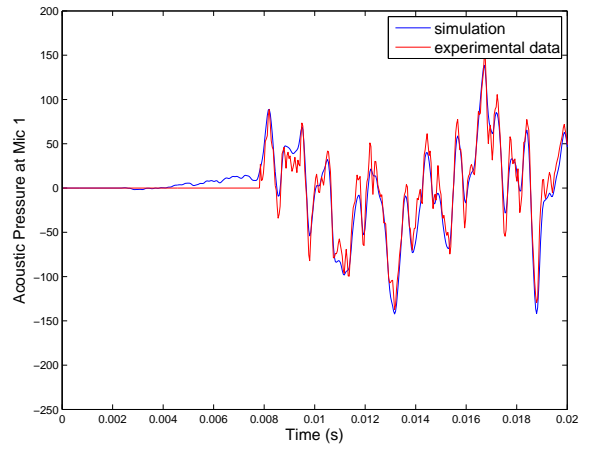
Figure 5 shows comparisons of the simulated and experimental acoustic pressures at microphones 1 and 2. The plots on the left show the entire time history, whereas the plots on the right show a closeup of the when the response first becomes non-zero. Good agreement is observed between the experimental and simulated data. Figure 6 shows closeups of different regions of the time histories for microphone 1. These figures show that good agreement is observed throughout the entire time history.

Figure 7 show similar results for microphones 3 and 4. Again, the agreement between experimental and simulated data is good. The remaining figures in the report show the same comparisons for the remaining 13 microphones. In all cases the matches are of a similar level of accuracy.

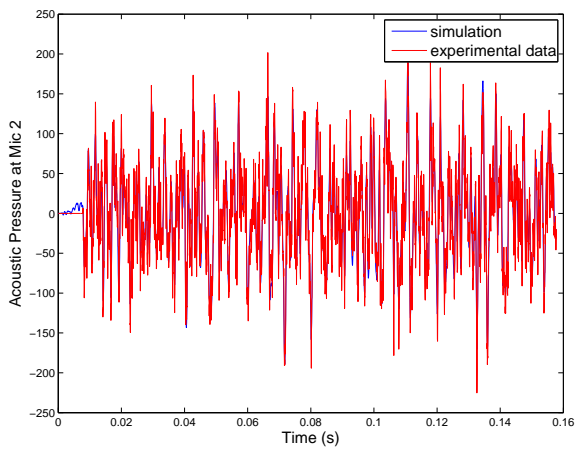
Finally, we examine the direct output of the inversion process to see if the results fall within the bounds expected from the physics of the problem. In Figure 15 we show the acoustic acceleration time histories, in  $\frac{m}{s^2}$ , for the first two patches in Figure 1. These acceleration time histories are the direct output of the inverse problem solution. The amplitudes of the inputs fall within the range of expected values, and do not show any unexpected behavior. However, more investigation is needed here, and a later report will investigate the patch results and accuracy metrics in more detail.



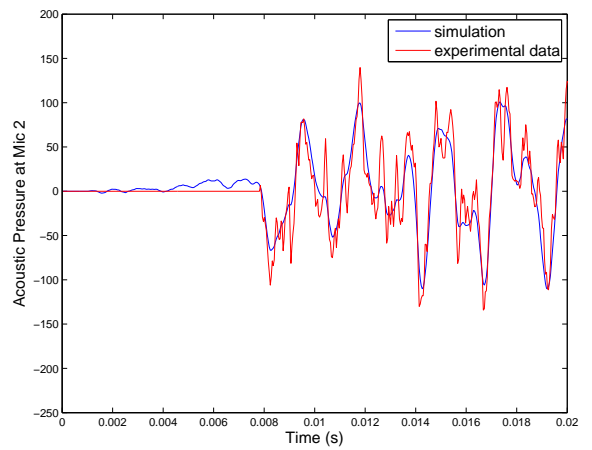
Acoustic pressures at microphone 1.



A closeup view of microphone 1.

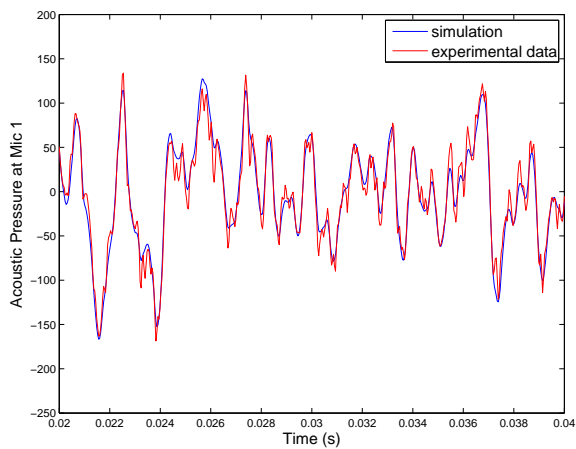


Acoustic pressures at microphone 2.

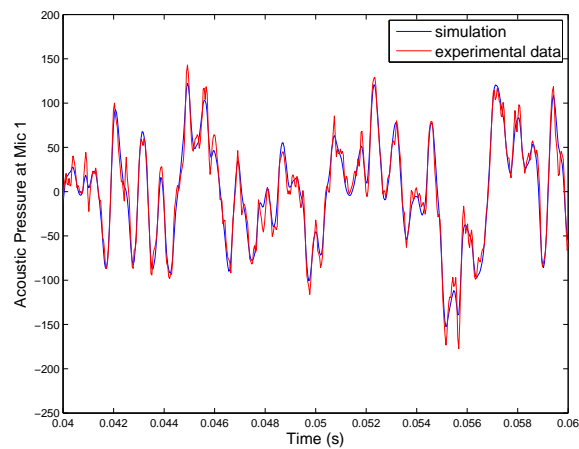


A closeup view of microphone 2.

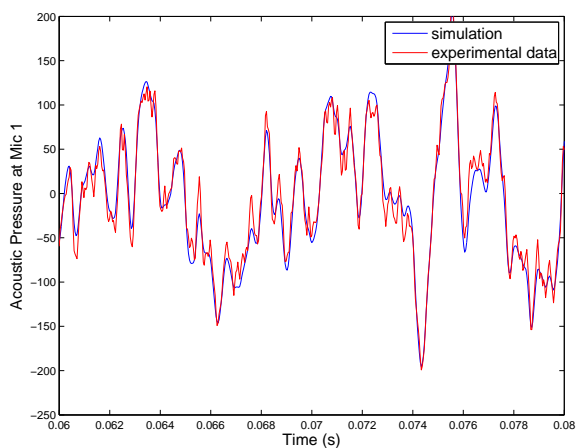
**Figure 5.** A comparison of measured and predicted acoustic pressures at microphones 1 and 2.



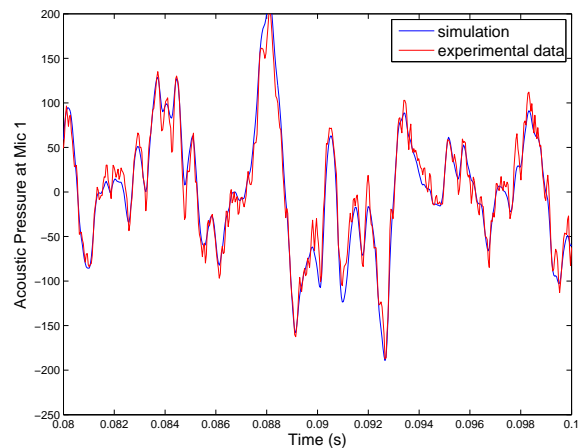
Time span from  $t = 0.02s$  to  $t = 0.04s$



Time span from  $t = 0.04s$  to  $t = 0.06s$

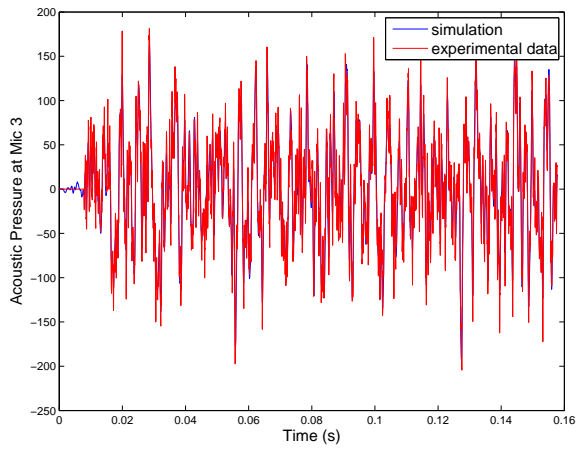


Time span from  $t = 0.06s$  to  $t = 0.08s$

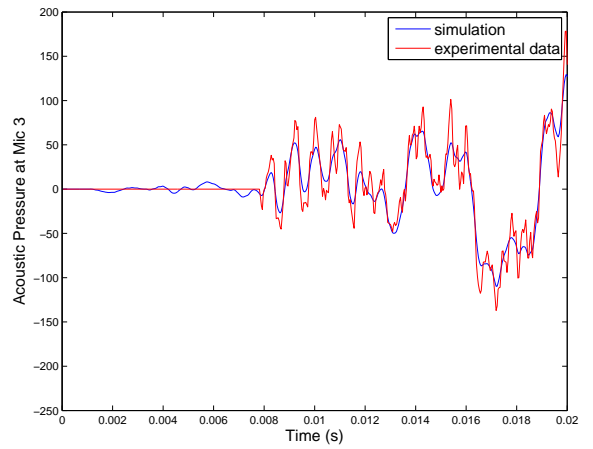


Time span from  $t = 0.08s$  to  $t = 0.1s$

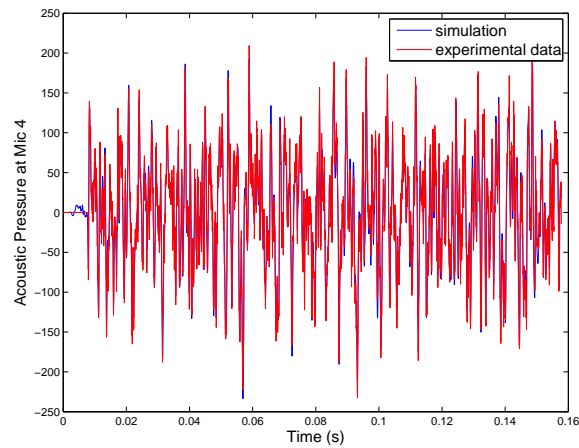
**Figure 6.** Closeup views of the time span from  $t = 0.02s$  to  $t = 0.1s$  of experimental and predicted acoustic pressures at microphone 1.



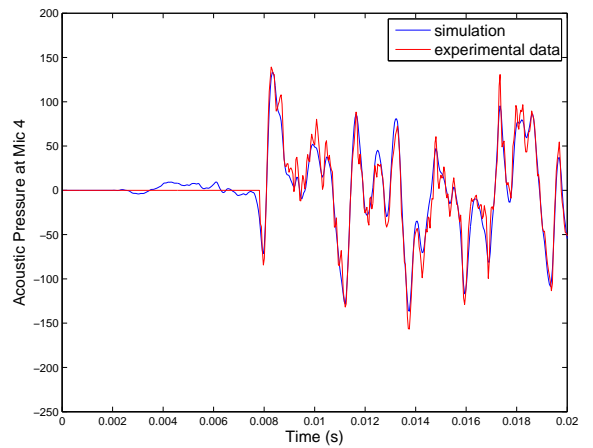
Acoustic pressures at microphone 3.



A closeup view of microphone 3.

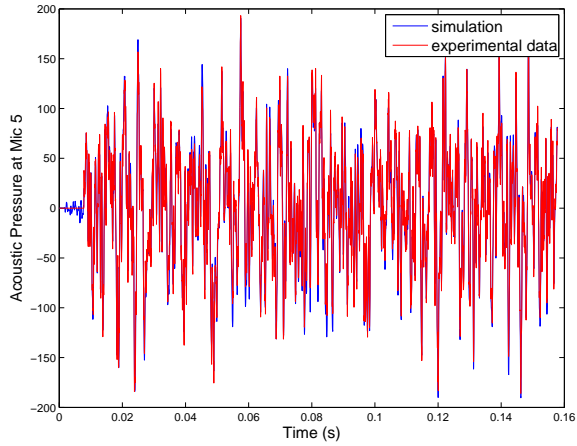


Acoustic pressures at microphone 4.

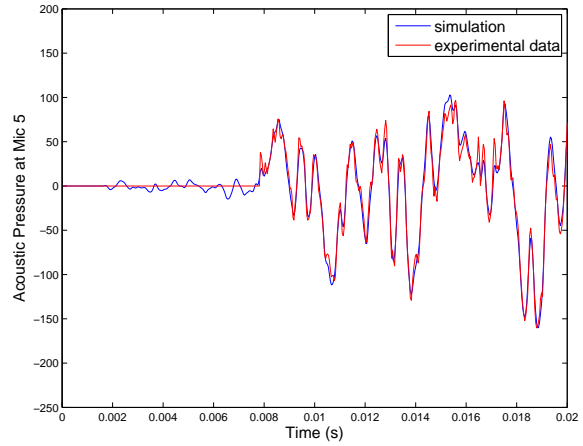


A closeup view of microphone 4.

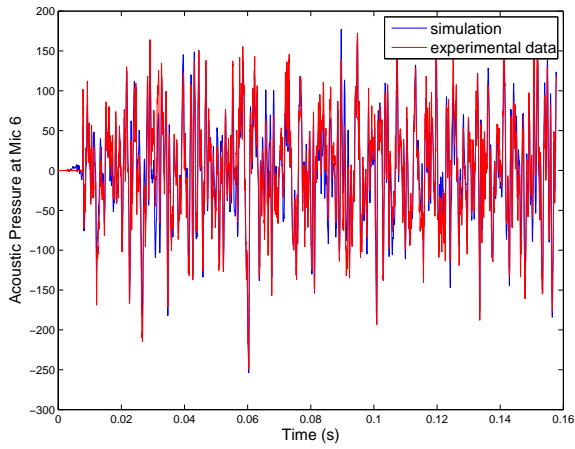
**Figure 7.** A comparison of experimental and predicted acoustic pressures at microphones 3 and 4.



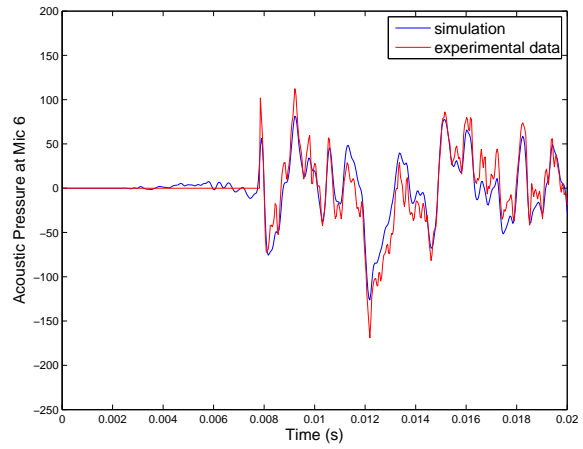
Acoustic pressures at microphone 5.



A closeup view of microphone 5.

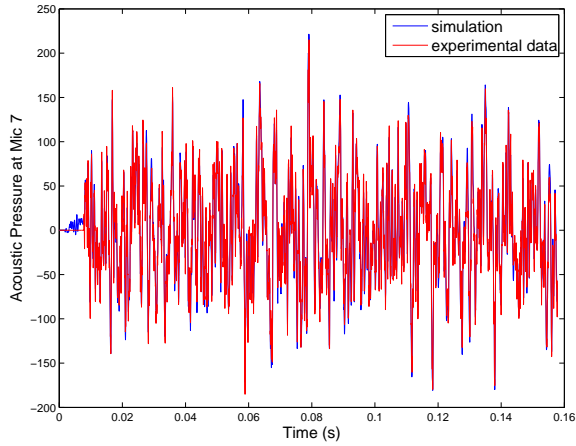


Acoustic pressures at microphone 6.

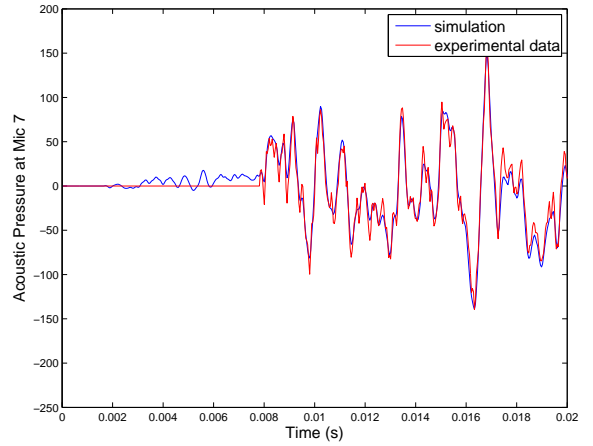


A closeup view of microphone 6.

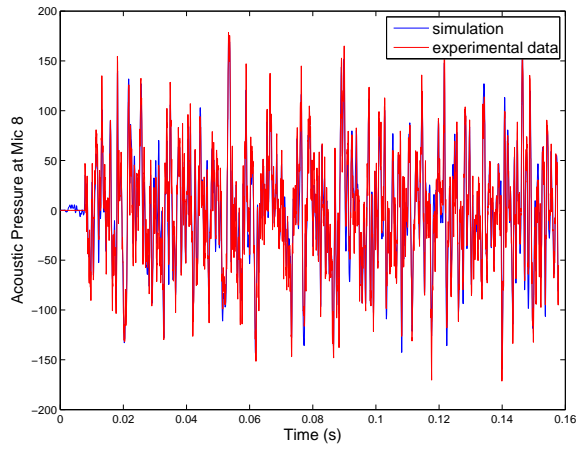
**Figure 8.** A closeup view of the early time comparison of experimental and predicted acoustic pressures at microphones 5 and 6.



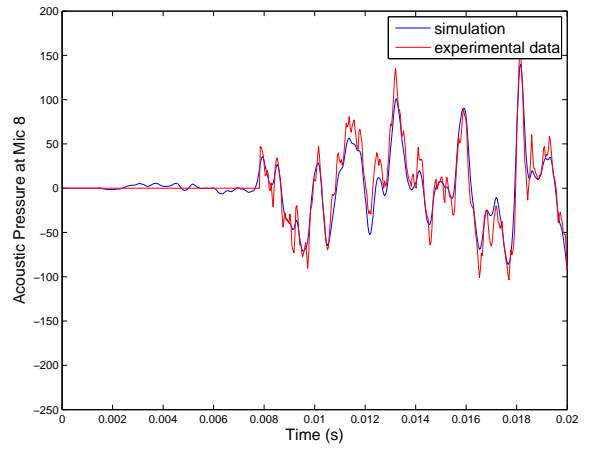
Acoustic pressures at microphone 7.



A closeup view of microphone 7.

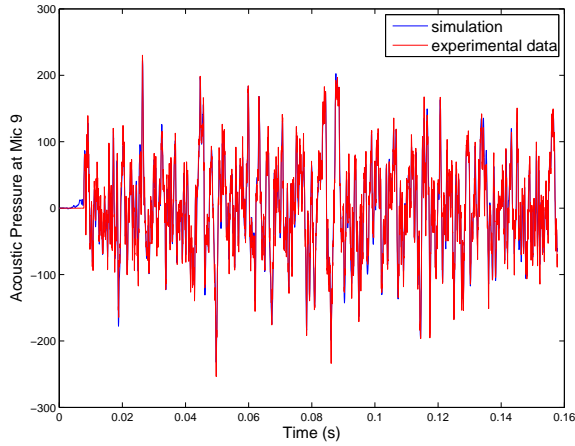


Acoustic pressures at microphone 8.

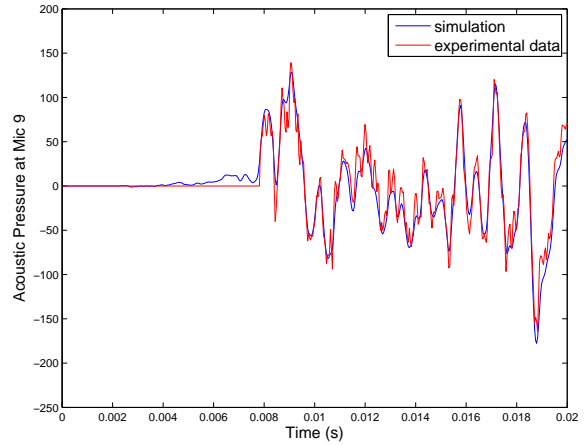


A closeup view of microphone 8.

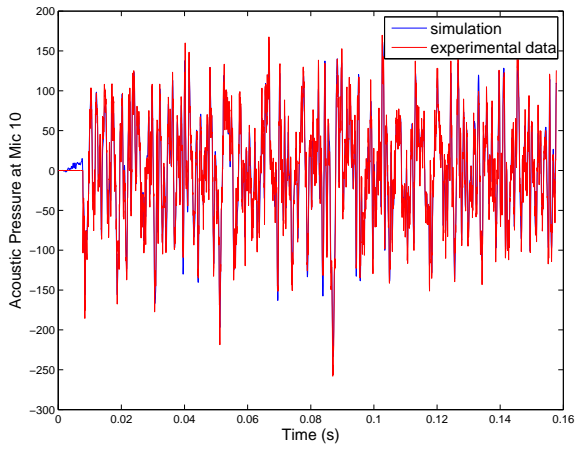
**Figure 9.** A closeup view of the early time comparison of experimental and predicted acoustic pressures at microphones 7 and 8.



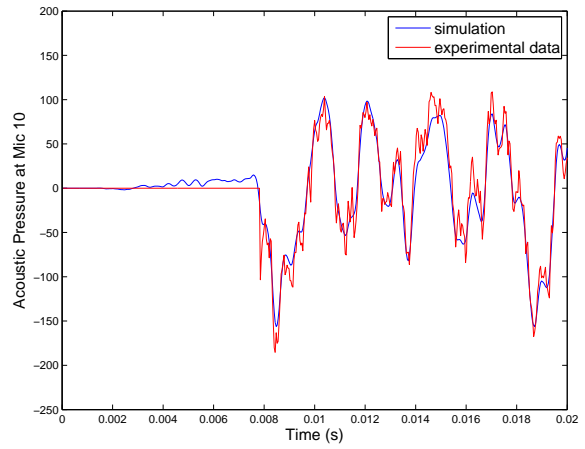
Acoustic pressures at microphone 9.



A closeup view of microphone 9.

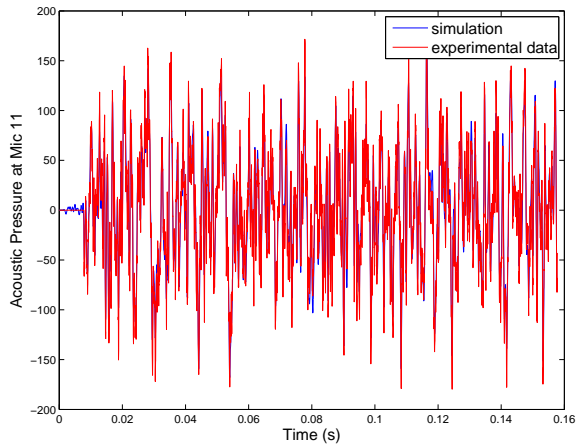


Acoustic pressures at microphone 10.

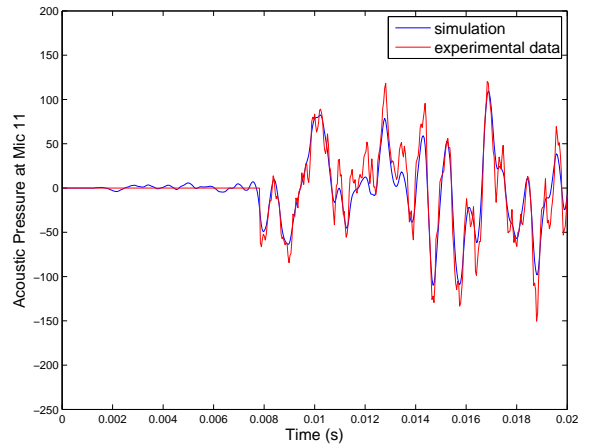


A closeup view of microphone 10.

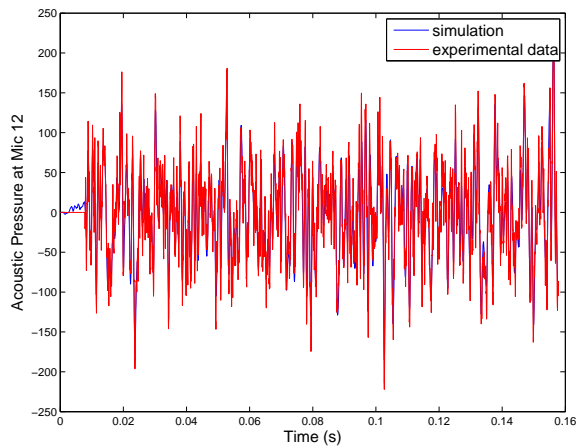
**Figure 10.** A closeup view of the early time comparison of experimental and predicted acoustic pressures at microphones 9 and 10.



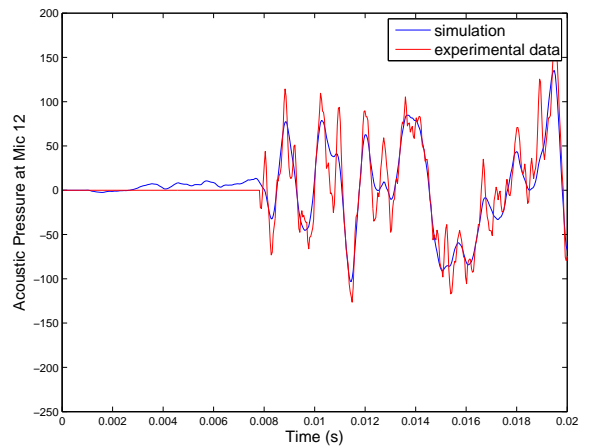
Acoustic pressures at microphone 11.



A closeup view of microphone 11.

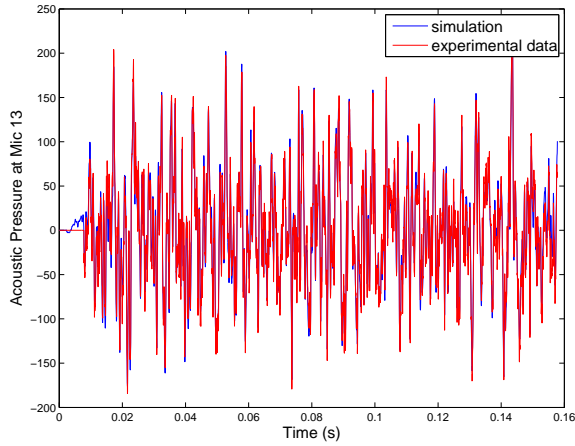


Acoustic pressures at microphone 12.

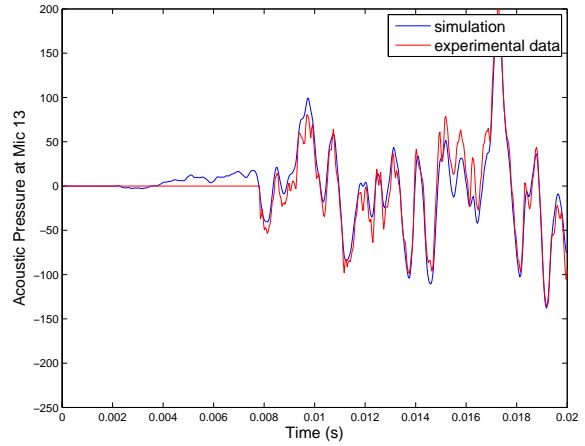


A closeup view of microphone 12.

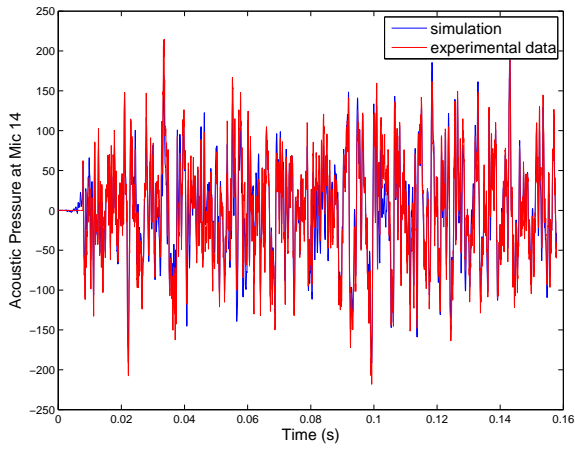
**Figure 11.** A closeup view of the early time comparison of experimental and predicted acoustic pressures at microphones 11 and 12.



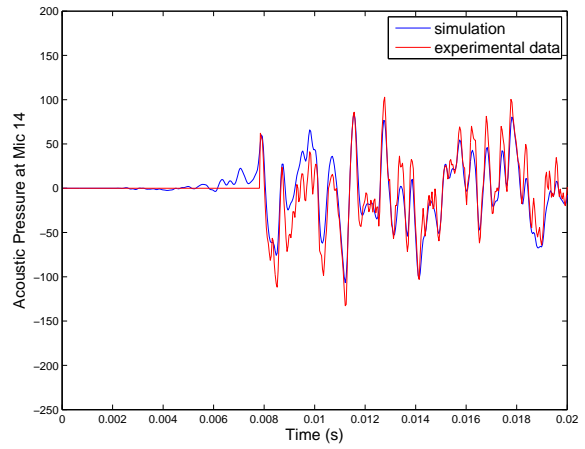
Acoustic pressures at microphone 13.



A closeup view of microphone 13.

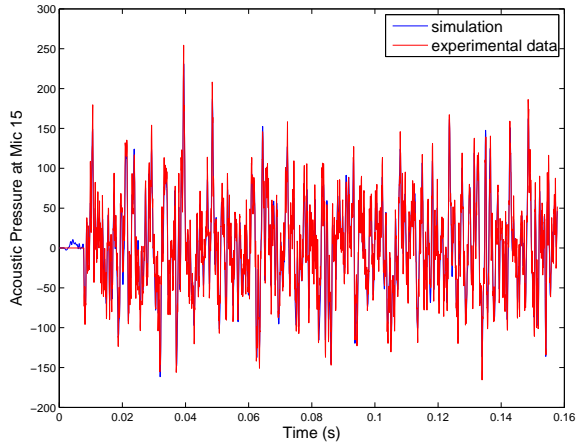


Acoustic pressures at microphone 14.

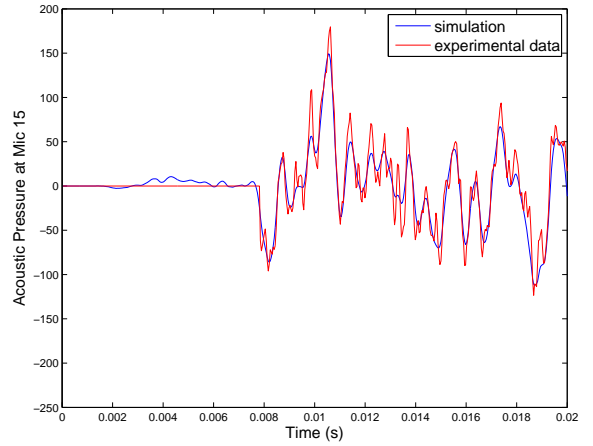


A closeup view of microphone 14.

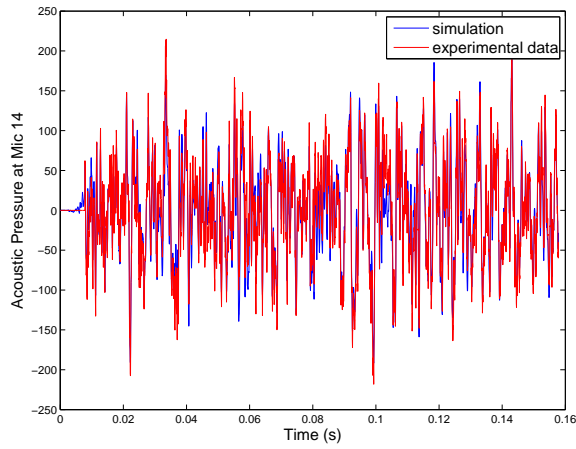
**Figure 12.** A closeup view of the early time comparison of experimental and predicted acoustic pressures at microphones 13 and 14.



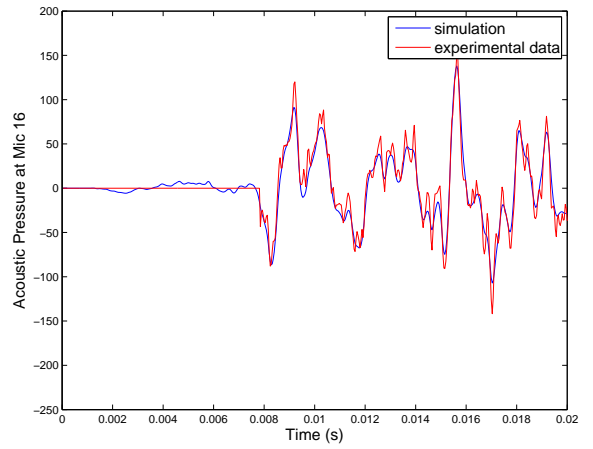
Acoustic pressures at microphone 15.



A closeup view of microphone 15.

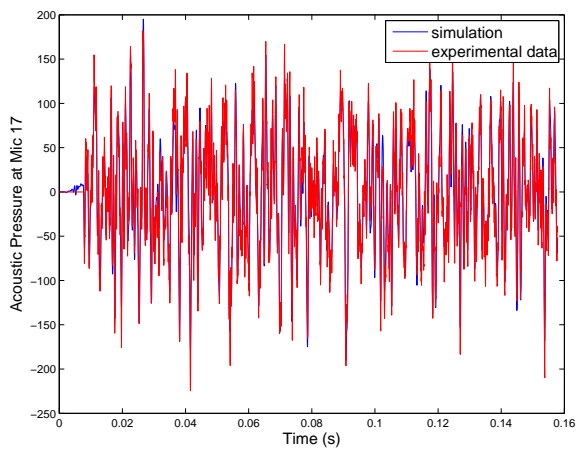


Acoustic pressures at microphone 16.

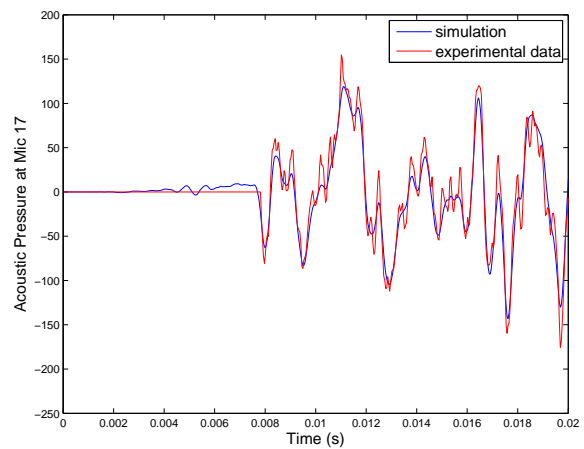


A closeup view of microphone 16.

**Figure 13.** A closeup view of the early time comparison of experimental and predicted acoustic pressures at microphones 15 and 16.

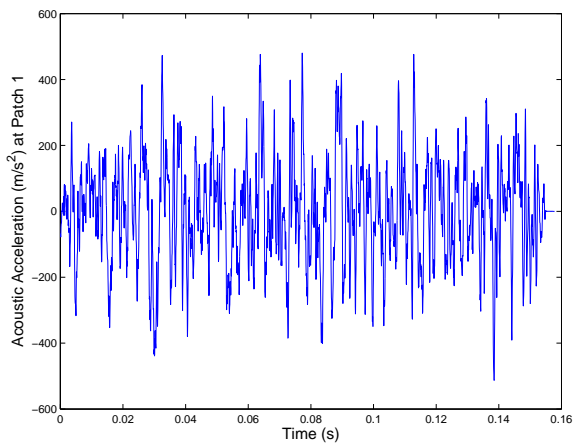


Acoustic pressures at microphone 17.

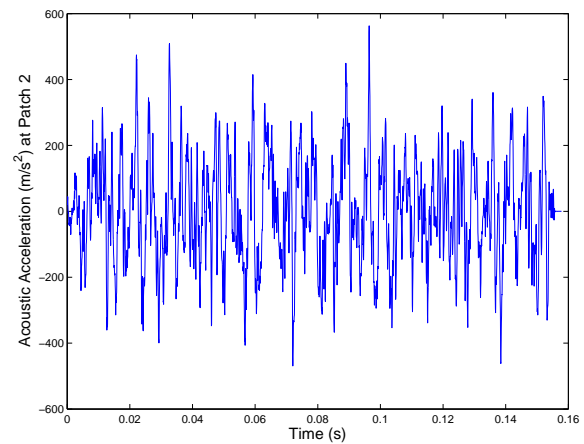


A closeup view of microphone 17.

**Figure 14.** A comparison of measured and predicted acoustic pressures at microphone 17.



patch 1



patch 2

**Figure 15.** Acoustic accelerations on first and second patches of Figure 1.

## 4 Conclusions

In this report, structural and acoustic source inversion algorithms have been presented in both time and frequency domains. These algorithms have been implemented in Sierra/SD with an interface to the Rapid Optimization Library (ROL). Gradients of the Lagrangian with respect to the design variables have been derived using the adjoint method, and explicit expressions for the gradient have been given in terms of the solution of the forward and adjoint problems. The minimization problems have been defined in terms of partial differential equation constrained optimization. A source inversion problem has been solved for a store flown on a military aircraft in both the time and frequency domains, corresponding to a recent experimental test in the reverberation chamber. The results of this source inversion problem were used to solve a forward problem to generate predicted microphone pressures for 17 microphones that were used in the experiment. Good agreement between the experimental measurements and the numerical simulations was observed, confirming that the inverse problem was solved to sufficient accuracy.

The next steps in this work are to examine the accuracy metrics for the inverse problem in more detail, and to examine the predictions of the forward problem for points that are away from the microphone measurement locations. The accuracy of these extrapolated predictions will depend on the number of measurement points and the number of patches. This work only solved the acoustic inverse problem, and so our current efforts involve extending the source inversion capability to coupled structural acoustics, which will include both the accelerometer data in the structure as well as the microphones. This will allow the algorithm to find patch inputs that drive the forward problem to match both the microphone and accelerometer measurements. In addition, we are extending the formulation to include second-order (Newton) methods, in order to compare the convergence behavior of first and second order approaches for this class of inverse problems.

## References

- [1] C. Larmat, J. Tromp, Q. Liu, and J. P. Montagner. Time reversal location of glacial earthquakes. *Journal of Geophysical Research*, 2002.
- [2] H. Kawakatsu and J. Montagner. Time reversal seismic source imaging and moment tensor inversion. *Geophys. J. Int.*, 2008.
- [3] R. Unnthorsson, T. Runarsson, and M. Jonsson. Acoustic emission based fatigue failure criterion for cfrp. *International Journal of Fatigue*, 2008.
- [4] A. Carpinteri, G. Lacidogna, and N. Pugno. Structural damage diagnosis and life-time assessment by acoustic emission monitoring. *Engineering Fracture Mechanics*, 2007.
- [5] O. E. Andreikiv, V. R. Skal's'kyi, and O. M. Serhienko. Acoustic-emission criteria for rapid analysis of internal defects in composite materials. *Materials Science*, 2001.
- [6] V. Akçelik, B. Biros, O. Ghattas, K. Long, and B. van Bloemen Waanders. A variational finite element method for source inversion for convective-diffusive transport. *Finite Elements in Analysis and Design*, 2003.
- [7] J. Benoit, C. Chauvière, and P. Bonnet. Source identification in time domain electromagnetics. *Journal of Computational Physics*, 231(8):3446 – 3456, 2012.
- [8] M. Fink, D. Cassereau, A. Derode, C. Prada, P. Roux, M. Tanter, J. L. Thomas, and F. Wu. Time-reversed acoustics. *Rep. Prog. Phys.*, 2000.
- [9] P. Blomgren, G. Papanicolaou, and H. Zhao. Super resolution in time-reversal acoustics. *Journal of the Acoustical Society of America*, 2002.
- [10] D. Jackson and D. Dowling. Phase conjugation in underwater acoustics. *J. Acoust. Soc. Am.*, 2007.
- [11] A. J. Devaney. Time reversal imaging of obscured targets from multistatic data. *IEEE Transactions on Antennas and Propagation*, 2005.
- [12] V. A. Zverev. The principle of acoustic time reversal and holography. *Acoustical Physics*, 2003.
- [13] J. Antoni. A bayesian approach to sound source reconstruction: Optimal basis, regularization, and focusing. *Journal of the Acoustical Society of America*, 2012.
- [14] D. P. Kouri, M. Heinkenschloss, D. Ridzal, and B.G. Van Bloemen Waanders. A trust-region algorithm with adaptive stochastic collocation for pde optimization under uncertainty. *Accepted with minor revisions, SIAM J. Sch. Comp.*, 2013.
- [15] G. Reese, M. Bhardwaj, and T. Walsh. Salinas- theory manual. Technical Report SAND2009-0748, Sandia National Labs, 2009.

- [16] T. J. R. Hughes. *The Finite Element Method: Linear Static and Dynamic Finite Element Analysis*. Prentice-Hall, 1987.
- [17] J. Nocedal and S. Wright. *Numerical Optimization*. Springer, 2006.
- [18] M. Heroux, R. Bartlett, V. Howle, R. Hoekstra, Hu J., T. Kolda, R. Lehoucq, K. Long, R. Pawlowski, E. Phipps, A. Salinger, H. Thornquist, R. Tuminaro, J. Willenbring, A. Williams, and K. Stanley. An overview of the trilinos project. *ACM Trans. Math. Softw.*, 31(3):397–423, 2005.
- [19] M. Cheney. The linear sampling method and the MUSIC algorithm. *Inverse Problems*, 2001.
- [20] J. Chen and R. Hudson. Source localization and beamforming. *IEEE Signal Processing Magazine*, 2002.
- [21] E. Marengo, F. Gruber, and F. Simonetti. Time-reversal MUSIC imaging of extended targets. *Image Processing, IEEE Transactions on*, 2007.
- [22] Y. D. Huang and M. Barkat. Near-field multiple source localization by passive sensor array. *IEEE Transactions on Antennas and Propagation*, 1991.
- [23] Q. Wang and F. Chu. Experimental determination of the rubbing location by means of acoustic emission and wavelet transform. *Journal of Sound and Vibration*, 2001.
- [24] A. Neumaier. Solving ill-conditioned and singular linear systems: a tutorial on regularization. *SIAM Rev.*, 1998.
- [25] G. Biros and O. Ghattas. Parallel lagrange newton krylov schur methods for pde-constrained optimization. part i: The krylov schur solver. *SIAM J. Sci. Comput.*, 2005.
- [26] G. Biros and O. Ghattas. Parallel lagrange newton krylov schur methods for pde-constrained optimization. part ii: The lagrange-newton solver and its application to optimal control of steady viscous flows. *SIAM J. Sci. Comput.*, 2005.
- [27] D Malioutov et. al. A sparse signal reconstruction perspective for source localization with sensor arrays. *IEEE Transactions on Signal Processing*, 2005.
- [28] X. Sheng and Y. Hu. Maximum likelihood multiple-source localization using acoustic energy measurements with wireless sensor networks. *IEEE Transactions on Signal Processing*, 2005.
- [29] H. Wang and P. Chu. Voice source localization for automatic camera pointing system in videoconferencing. In *Applications of Signal Processing to Audio and Acoustics 1997. 1997 IEEE ASSP Workshop On*, 1997.
- [30] D. Bechler, M. S. Schlosser, and Kroschel K. System for robust 3d speaker tracking using microphone array measurements. In *Intelligent Robots and Systems 2004, (IROS 2004). Proceedings. 2004 IEEE/RSJ International Conference on*, 2004.

- [31] S. T. Birchfield. A unifying framework for acoustic source localization. In *Proceedings of the 12th European Signal Processing Conference*, 2004.
- [32] et. al. Warsitz, E. Adaptive beamforming combined with particle filtering for acoustic source localization. In *International conference on spoken language*, 2004.
- [33] M. Fink. Time-reversal acoustics. In *Journal of Physics: Conference Series*, 2008.
- [34] M. Bhardwaj, K. Pierson, G. Reese, T. Walsh, D. Day, K. Alvin, J. Peery, C. Farhat, and M. Lesoinne. Salinas: a scalable software for high-performance structural and solid mechanics simulations. In *Supercomputing, ACM/IEEE 2002 Conference*, pages 35–35. IEEE, 2002.
- [35] C. Zhu, R. H. Byrd, P. Lu, and J. Nocedal. Algorithm 778: L-bfgs-b: Fortran subroutines for large-scale bound-constrained optimization. *ACM Transactions on Mathematical Software (TOMS)*, 23(4):550–560, 1997.
- [36] R. E. Plessix. A review of the adjoint-state method for computing the gradient of a functional with geophysical applications. *Geophysical Journal International*, 167(2):495–503, 2006.
- [37] M. Sambridge and K. Mosegaard. Monte carlo methods in geophysical inverse problems. *Reviews of Geophysics*, 40(3):1009, 2002.
- [38] V. Isakov. *Inverse problems for partial differential equations*, volume 127. Springer Verlag, 1998.
- [39] S. Boyd and L. Vandenberghe. *Convex optimization*. Cambridge university press, 2004.
- [40] L. T. Biegler. *Large-scale PDE-constrained optimization*, volume 30. Springer Verlag, 2003.

## DISTRIBUTION:

2 MS 9018      Central Technical Files, 8944

2 MS 0899      Technical Library, 4536





